Journal of Radiation Research, Vol. 59, No. 6, 2018, pp. 782–788
doi: 10.1093/jrr/rry062
Advance Access Publication: 14 August 2018

Relationship between pressure levels on the occipital region and intrafraction motion using an individualized head support for intracranial treatment

Hiroki Inata[1,*], Yuta Kuribayashi[1], Azusa Katakami[1], Noritaka Sodeoka[1], Shigeki Nakayama[1] and Osamu Nishizaki[2]

[1]Department of Radiology, Saiseikai Imabari Hospital, 7-1-6 Kitamura, Imabari, Ehime, 799-1592, Japan
[2]Department of Neurosurgery, Saiseikai Imabari Hospital, 7-1-6 Kitamura, Imabari, Ehime, 799-1592, Japan
*Corresponding author. Department of Radiology, Saiseikai Imabari Hospital, 7-1-6 Kitamura, Imabari, Ehime, 799-1592, Japan, Tel: +81-898-47-6019; Fax: +81-898-47-5096; Email: inata.hiroki@gmail.com
(Received 7 September 2017; revised 14 June 2018; editorial decision 7 July 2018)

ABSTRACT

The purpose of this study was to evaluate the relationship between pressure on the occipital region and intrafraction motion using an individualized vacuum pillow and a thermoplastic mask for intracranial treatment. We calculated head displacement during treatment from 8811 image verifications in 59 patients and divided them into two groups according to the magnitude of the mean and standard deviation (SD) of the displacement in the 59 patients. Pressure was compared between the small ($n = 29$) and large ($n = 30$) displacement groups using Welch's *t*-test for the mean and SD of displacement. The mean head displacement in the small and large groups was (0.3, 0.3, 0.4) and (0.5, 0.6, 0.7) (unit: mm) for the vector length and 10 mm and 30 mm radius targets, respectively. The mean SD of head displacement in the small and large groups was (0.2, 0.2, 0.2) and (0.3, 0.3, 0.4) (unit: mm) for the vector length and 10 mm and 30 mm radius targets, respectively. Significant differences were observed in the SD of the displacement in the vector length and 10 mm radius target between the two groups. The SD of the displacement under a pressure of 15 kPa was smaller than that under a pressure of 11 kPa. The intrafraction motion under a high-pressure level on the occipital region was less than that under a low-pressure level. Management of pressure on the occipital region may result in less intrafraction motion in clinical practice.

Keywords: immobilization; pressure; intrafraction motion; head; IGRT

INTRODUCTION

Stereotactic radiosurgery (SRS) and stereotactic radiotherapy (SRT) have become widely used because they can irradiate the target with a large dose and decrease the dose to normal tissue in comparison with whole-brain radiation therapy. Recently, Linac-based SRS and SRT using a frameless system with an image-guided radiation therapy (IGRT) technique have been implemented in the intracranial region [1–6], since image diagnosis techniques have been rapidly improving. Although the frameless system with IGRT has achieved high positioning accuracy, some researchers have reported that the intrafraction motion of the intracranial region can be >1 mm [7–11]. In addition, the frameless system with IGRT is considered to be less accurate than invasive frame-based systems [10, 12].

To decrease intrafraction motion using a frameless system with IGRT in SRS and SRT, we consider that the following steps should be performed: (i) acquiring more frequency in the image registration, (ii) using immobilization devices with high positioning accuracy and (iii) decreasing patient discomfort. To address the first issue, imaging devices that can detect the patient position in

real-time have been developed [13–24]. Regarding the second issue, many commercially available immobilization devices with high positioning accuracy have been introduced. Finally, to address the third issue, a customized head and neck support is considered to be beneficial because it increases the comfort of the patient during treatment, resulting in less patient movement [25]. Since a customized head and neck support that fits to the patient's occipital shape creates uniform pressure on the patient's head, the patient feels negligible discomfort [26–29]. However, the uniformity of pressure on the patient's head can be lost due to mask shrinkage or deformation of the head and neck support (e.g. shrinkage or expansion, air leakage) in proportion to the time passed since molding in clinical application [30]. Therefore, management of the uniform pressure on the patient's head is important for improving positioning accuracy. Changes in the uniform pressure may cause patient discomfort and weakening of the fixation of patient. Hence, specific methods for maintaining the uniformity of the pressure on the patient's head may lead to high positioning accuracy in intracranial treatments.

The purpose of this study was to evaluate the relationship between pressure on the occipital region and intrafraction motion using an individualized vacuum pillow and a thermoplastic mask in intracranial treatments.

MATERIALS AND METHODS

This retrospective study was approved by our institutional review board (Approval number: I28–12).

We used a frameless system that consists of an individualized vacuum pillow (YCI-01, Engineering System, Matsumoto, Japan), a thermoplastic mask (RT-1779KS, Qfix, PA, USA) and a baseplate (MT-20 108, CIVCO, IA, USA) (Fig. 1). The vacuum pillow could be customized to the patient's occipital shape to create uniform pressure on the patient's head. We also used a dedicated real-time monitoring system [16] that consisted of pressure sensors (FSR®402, Interlink Electronics, CA, USA) with a thickness of 0.6 mm and a radius of 9.1 mm to detect the pressure on the patient's head. Four sensors are able to detect the absolute pressures at the occipital region as voltages, with a sampling rate of 15 s^{-1}. They can detect a range from 0 to 90 kPa, with a resolution of 1.3 Pa. This system has several advantages: high sensitivity, low cost, low invasion, thin and small size, easy application, and simple measurement. It can also detect the vector length of intrafraction motion without radiation exposure to the patient.

A total of 59 patients (40 males and 19 females) were treated in the intracranial region using the Cyberknife (Accuray, CA, USA) system between May 2013 and December 2017, and they all provided informed consent. Their median age was 68.0 years (range: 26–87 years). The patient's head displacement was determined at 63 s intervals by a Target Locating System (TLS, Accuray, CA, USA), which can detect head position precisely with orthogonal X-ray images. The registration errors on TLS were 0.33 ± 0.16 mm (mean ± 1 SD) in the overall translation and 0.29°± 0.11°(mean ± 1 SD) in the overall rotation [31]. We calculated the head displacement detected by TLS and the mean pressure of the four sensors from 8811 image verifications with 263 treatments. When a patient is moved by a radiation therapist for repositioning, the head position will be completely different from the head position at the beginning of treatment, resulting in overestimation of the head displacement. Therefore, head displacement was excluded when a patient was moved.

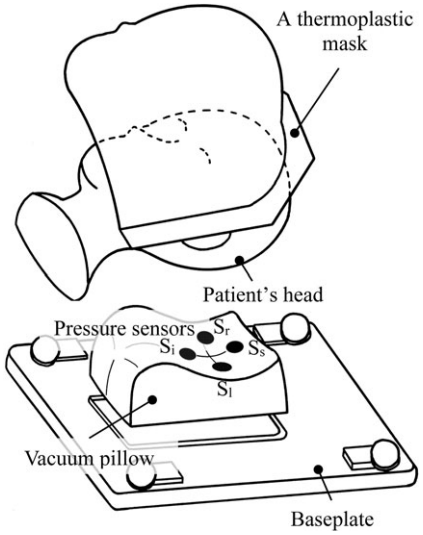

Fig. 1. A vacuum pillow (YCI-01, Engineering System, Nagano, Japan), a thermoplastic mask (RT-1779KS, Qfix, PA, USA), a baseplate (MT-20108, CIVCO, IA, USA) and four pressure sensors (FSR®402, Interlink Electronics, CA, USA). The vacuum pillow can be customized to the patient's occipital shape. Four sensors can detect the absolute pressures on the occipital region, with a sampling rate of 15 s^{-1}. They can also detect at a range from 0 to 90 kPa with a resolution of 1.3 Pa.

To calculate the magnitude of head displacement, the absolute changes in head displacement detected by TLS, $\Delta d_{TLS}(t)$, during treatment was defined as follows:

$$\Delta d_{TLS}(t) = |d_{TLS}(t) - d_{TLS}(t_0)|, \quad (1)$$

where $d_{TLS}(t_0)$ and $d_{TLS}(t)$ are the displacements detected at the beginning of the treatment t_0 and at time t, respectively. Time t corresponds to the time of TLS acquisition during treatment. $\Delta d_{TLS,SI}(t)$, $\Delta d_{TLS,RL}(t)$ and $\Delta d_{TLS,AP}(t)$ are the displacements in the SI direction, RL direction and AP direction, respectively. The vector length of the displacement, $\Delta d_V(t)$, during treatment was defined as follows:

$$\Delta d_V(t) = \sqrt{\Delta d^2_{TLS,SI}(t) + \Delta d^2_{TLS,RL}(t) + \Delta d^2_{TLS,AP}(t)} \quad (2)$$

The patient positioning error increases in proportion to the rotation angle and the distance between the imaging center and the target

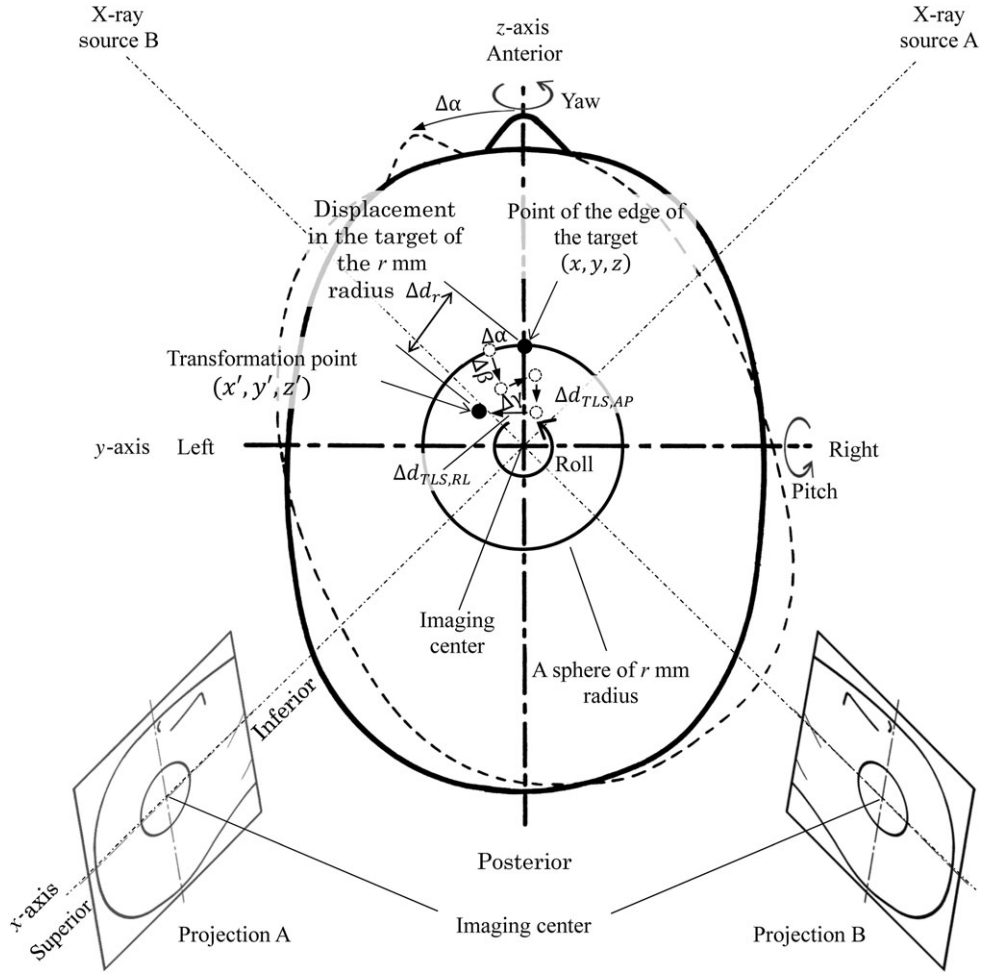

Fig. 2. A diagram of the concept of the patient positioning error. The displacements on the *x*, *y* and *z*-axes are $\Delta d_{TLS,SI}$, $\Delta d_{TLS,RL}$ and $\Delta d_{TLS,AP}$, respectively. Similarly, the displacements in the rotational angles on the *x*, *y* and *z*-axes are roll ($\Delta\alpha$), pitch ($\Delta\beta$), and yaw ($\Delta\gamma$), respectively. The point of the edge of the target, (x, y, z), was rotated around the imaging center by $\Delta\alpha - \Delta\beta - \Delta\gamma$, then the transformation point, (x', y', z'), was established by subtracting ($\Delta d_{TLS,SI}$, $\Delta d_{TLS,RL}$, $\Delta d_{TLS,AP}$) from this rotated point. The displacement in the target of the *r* mm radius, Δd_r, is a vector length between the edge of the target and the transformation point, which is corrected by the translational and rotational displacement.

position [32]. A conceptual diagram of the patient positioning error is shown in Fig. 2. The distance between the imaging center and the edge of the target increases depending on the target size. Therefore, the point of the edge of the target, (x, y, z), was set to the surface of a sphere. (x, y, z) was expressed as follows:

$$x^2 + y^2 + z^2 = r^2, \tag{3}$$

where r is the target radius, which was set to 10 mm and 30 mm because an arteriovenous malformation of more than 30 mm radius was treated according to the SRT protocol in our institution. The displacements of the rotational angles in the x, y and z-axes were roll, $\Delta\alpha(t)$, pitch, $\Delta\beta(t)$, and yaw, $\Delta\gamma(t)$, respectively. (x, y, z) was transformed into $[x'(t), y'(t), z'(t)]$ by the rotation matrix with roll, pitch and yaw angles as follows:

$$\begin{pmatrix} x'(t) \\ y'(t) \\ z'(t) \end{pmatrix} = \begin{pmatrix} \cos\Delta\gamma(t) & \sin\Delta\gamma(t) & 0 \\ -\sin\Delta\gamma(t) & \cos\Delta\gamma(t) & 0 \\ 0 & 0 & 1 \end{pmatrix} \times \begin{pmatrix} \cos\Delta\beta(t) & 0 & -\sin\Delta\beta(t) \\ 0 & 1 & 0 \\ \sin\Delta\beta(t) & 0 & \cos\Delta\beta(t) \end{pmatrix} \times \begin{pmatrix} 1 & 0 & 0 \\ 0 & \cos\Delta\alpha(t) & \sin\Delta\alpha(t) \\ 0 & -\sin\Delta\alpha(t) & \cos\Delta\alpha(t) \end{pmatrix} \begin{pmatrix} x \\ y \\ z \end{pmatrix} - \begin{pmatrix} \Delta d_{TLS,SI}(t) \\ \Delta d_{TLS,RL}(t) \\ \Delta d_{TLS,AP}(t) \end{pmatrix} \tag{4}$$

The transformation point, $(x'(t), y'(t), z'(t))$ is corrected for 6-D displacements of the position and rotation. Therefore, the displacement in the target of the r mm radius, $\Delta d_r(t)$ was obtained from Equations (3) and (4) as follows:

$$\Delta d_r(t) = \sqrt{(x - x'(t))^2 + (y - y'(t))^2 + (z - z'(t))^2}, \quad (5)$$

where, x, y and z are defined unambiguously by the maximum value of $\Delta d_r(t)$.

On the other hand, the mean pressure of four sensors, $\bar{P}(t)$, during treatment is defined as follows:

$$\bar{P}(t) = \frac{P_S(t) + P_I(t) + P_R(t) + P_L(t)}{4}, \quad (6)$$

where $P_S(t)$, $P_I(t)$, $P_R(t)$ and $P_L(t)$ are the pressures at the superior side, inferior side, right side and left side on the vacuum pillow at the time of TLS acquisition during treatment, t, respectively.

$\Delta d_V(t)$, $\Delta d_r(t)$ and $\bar{P}(t)$ were calculated at every treatment. Then we divided the results into two groups according to the magnitude of the mean and the standard deviation (SD) of displacement in 59 patients. The mean pressures were compared between the small ($n = 29$) and large ($n = 30$) displacement groups using Welch's t-test for the mean and SD of the displacements. All P-values were two sided, and P-values of ≤ 0.05 were considered to be significant. All statistical analyses were performed with EZR [33] (Saitama Medical Center, Jichi Medical University, Saitama, Japan), which is a graphical user interface for R (The R Foundation for Statistical Computing, Vienna, Austria). Cohen's d (Effect size) and $1 - \beta$ error probability (Power) for t-tests was performed by G*Power3.1 [34, 35].

RESULTS

Table 1 shows the displacement and pressure in the large and small groups separated based on the magnitude of the mean displacement. The mean displacement in the small and large groups was (0.3, 0.3, 0.4) and (0.5, 0.6, 0.7) (unit: mm) for the vector length and 10 mm and 30 mm radius targets, respectively. Similarly, the mean pressure of the mean displacement in the small and large groups was (14.5, 14.5, 14.2) and (11.5, 11.5, 11.8) (unit: kPa) for the vector length 10 mm and 30 mm radius targets, respectively. There was no significant difference in the mean displacement.

Table 2 shows the displacement and pressure in the large and small groups separated based on the magnitude of the mean of the SD of the displacement. The mean of the SD of the displacement in the small and large groups was (0.2, 0.2, 0.2) and (0.3, 0.3, 0.4) (unit: mm) for the vector length and 10 mm and 30 mm radius targets, respectively. Similarly, the mean pressure of the SD of the displacement in the small and large groups was (15.2, 15.4, 14.8) and (10.8, 10.6, 11.2) (unit: kPa) for the vector length and 10 mm and 30 mm radius targets, respectively. The mean of the SD of the displacement under high pressure was smaller than that under low pressure, and a significant difference was seen in the SD of the displacement for the vector length and the 10 mm radius target.

DISCUSSION

The SD of the displacement under high pressure was smaller than that under low pressure for the vector length and 10 mm radius target. These results were consistent with our previous findings using a head phantom to evaluate the positioning accuracy of a frameless system. On the other hand, there was no significant difference in the mean displacement. The mean and the SD of the displacement mainly represent head movement that increases with time, and head movement over a short period, respectively. Maintaining a high pressure level on the occipital region might be more effective at maintaining positioning accuracy over a short period than that of reducing cumulative head movement. A possible explanation for this is that the force of the head movement in a short time given to the immobilization devices is stronger than that in a long time. Since the SD of the displacement represents random variations, random variations could be reduced by maintaining a high-pressure level on the patient's occipital region during treatment. A pressure of 15 kPa on the occipital region could result in less intrafraction motion and prevent abrupt or respiratory motion in clinical practice. An adjustable thickness spacer that could compensate for mask loosening or shrinkage [36] might be useful for maintaining a high-pressure level on the patient's occipital region in clinical application.

Table 1. The displacement and the pressure in the two groups separated based on the magnitude of the mean displacement

	Group	Mean pressure (kPa)		Mean displacement (mm)		*P*-value	Effect size	Power
		Mean	SD	Mean	SD			
Vector length	Small ($n = 29$)	14.5	6.9	0.27	0.05	0.109	0.42	0.35
	Large ($n = 30$)	11.5	7.0	0.47	0.09			
10 mm radius target	Small	14.5	6.9	0.31	0.05	0.109	0.42	0.35
	Large	11.5	7.0	0.55	0.10			
30 mm radius target	Small	14.2	6.7	0.41	0.07	0.193	0.34	0.25
	Large	11.8	7.2	0.73	0.14			

There was no significant difference in the mean displacement. n = number of patients, Mean = mean value, SD = standard deviation, Effect size = Cohen's d, Power = $1 - \beta$ error probability.

Table 2. The displacement and the pressure in the two groups separated based on the magnitude of the mean of the standard deviation (SD) of the displacement

	Group	Mean pressure (kPa)		SD of displacement (mm)		*P*-value	Effect size	Power
		Mean	SD	Mean	SD			
Vector length	Small ($n = 29$)	15.2	7.6	0.15	0.02	0.017	0.64	0.68
	Large ($n = 30$)	10.8	5.7	0.28	0.13			
10 mm radius target	Small	15.4	7.5	0.16	0.02	0.009	0.71	0.76
	Large	10.6	5.7	0.31	0.14			
30 mm radius target	Small	14.8	7.2	0.20	0.03	0.052	0.52	0.50
	Large	11.2	6.5	0.40	0.17			

A significant difference was seen in the SD of the displacement for the vector length and the 10 mm radius target. n = number of patients, Mean = mean value, SD = standard deviation, Effect size = Cohen's d, Power = 1 – β error probability.

The intrafraction motion under a low-pressure level was 0.47 ± 0.28 mm (mean ± 1 SD) for the vector length. Ramakrishna [10] reported that intrafraction motion was 0.7 ± 0.5 mm (mean ± 1 SD), and Verbakel [4] reported that intrafraction motion was 0.35 ± 0.21 mm (mean ± 1 SD). The magnitude of the intrafraction motion in these reports was almost the same as that of our study. If treatment is performed with a pressure of >15 kPa on the occipital region, intrafraction motion will be <0.27 ± 0.15 mm (mean ± 1 SD). Similarly, intrafraction motion under a low- and high-pressure level was 0.73 ± 0.40 mm and 0.41 ± 0.20 mm for the 30 mm radius target. Those values are larger than that for the vector length. Hence, the pressure on the occipital region under a high-pressure level may improve positioning accuracy, depending on the target size.

When a patient's head was fixed with a high pressure, the vacuum pillow and the thermoplastic mask were deformed at a millimeter or submillimeter scale, resulting in spreading of the high-pressure area and uniformity of pressure across the vacuum pillow. As the high-pressure area becomes larger, fixation of the patient's head becomes stronger. However, a few sensors could not detect the pressure on the occipital region because there may have been some small air gaps between the head and the vacuum pillow. It is important to reduce these air gaps by being careful with pillow molding and patient positioning.

The dimensions of the hollow pillow were a sphere with an approximate radius of 5 cm and a depth of 2 cm. Since the contact area between the occipital region and the vacuum pillow was 63 cm^2, a force of 94 N (= 9.6 kgf) might be expected by applying a pressure of 15 kPa against the occipital region. Thus, patients might be restricted by a force of 90 N during treatment when the intrafraction motion is 0.27 ± 0.15 mm. On the other hand, the force might be <90 N because there could be some small air gaps between the occipital region and the vacuum pillow, as mentioned above.

The present study showed that the positioning accuracy for the intracranial region could be improved by applying a pressure of 15 kPa on the patient's occipital region in clinical application. However, the patient may feel uncomfortable with the increased force of immobilization. In view of this, further study is necessary to find what would be a reasonable pressure level for the occipital region.

CONCLUSION

The SD of the displacement under a high-pressure level was smaller than that under a low-pressure level. A high-pressure level on the occipital region may improve the positioning accuracy, depending on the target size. Management of the pressure on the occipital region may result in less intrafraction motion and prevent abrupt or respiratory motion in clinical practice.

ACKNOWLEDGEMENTS

This study was presented orally at the 111th Scientific Meeting of the Japan Society of Medical Physics in Yokohama, Japan (April 2016). The authors would like to thank Professor Fujio Araki of Kumamoto University and Dr Yuji Nakaguchi of Kumamoto University Hospital for their helpful suggestions, and Dr Hirofumi Oohashi of Accuray Japan K.K. for providing technical information about the Cyberknife system. The authors also thank Dr Yasushi Hamamoto of Ehime University for his thoughtful comments on this research.

CONFLICT OF INTEREST

The authors state that there are no conflicts of interest.

FUNDING

This study was supported by a Grant-in-aid for research on radiation oncology of Japanese Society for Radiation Oncology (JASTRO) 2014–2015.

REFERENCES

1. Ryken TC, Meeks SL, Pennington EC et al. Initial clinical experience with frameless stereotactic radiosurgery: analysis of accuracy and feasibility. *Int J Radiat Oncol Biol Phys* 2001;51: 1152–8.
2. Feygelman V, Walker L, Chinnaiyan P et al. Simulation of intrafraction motion and overall geometrical accuracy of a frameless intracranial radiosurgery process. *J Appl Clin Med Phys* 2008;9: 68–86.
3. Breneman JC, Steinmetz R, Smith A et al. Frameless image-guided intracranial stereotactic radiosurgery: clinical outcomes for brain metastases. *Int J Radiat Oncol Biol Phys* 2009;74: 702–6.
4. Verbakel WFAR, Lagerwaard FJ, Verduin AJE et al. The accuracy of frameless stereotactic intracranial radiosurgery. *Radiother Oncol* 2010;97:390–4.
5. Wiersma RD, Wen Z, Sadinski M et al. Development of a frameless stereotactic radiosurgery system based on real-time 6D position monitoring and adaptive head motion compensation. *Phys Med Biol* 2010;55:389–401.
6. Minniti G, Scaringi C, Clarke E et al. Frameless linac-based stereotactic radiosurgery (SRS) for brain metastases: analysis of patient repositioning using a mask fixation system and clinical outcomes. *Radiat Oncol* 2011;6:158.
7. Murphy M, Chang S, Gibbs I et al. Patterns of patient movement during frameless image-guided radiosurgery. *Int J Radiat Oncol* 2003;55:1400–8.
8. Hoogeman MS, Nuyttens JJ, Levendag PC et al. Time dependence of intrafraction patient motion assessed by repeat stereoscopic imaging. *Int J Radiat Oncol Biol Phys* 2008;70:609–18.
9. Saito K, Fujii M, Kajiwara K et al. Introducing sitetrack: continuous patient motion monitoring during stereotactic radiotherapy for the head. *Neurosurgery* 2009;64:A110–22.
10. Ramakrishna N, Rosca F, Friesen S et al. A clinical comparison of patient setup and intra-fraction motion using frame-based radiosurgery versus a frameless image-guided radiosurgery system for intracranial lesions. *Radiother Oncol* 2010;95:109–15.
11. Kang H, Lovelock DM, Yorke ED et al. Accurate positioning for head and neck cancer patients using 2D and 3D image guidance. *J Appl Clin Med Phys* 2011;12:3270.
12. Kumar S, Burke K, Nalder C et al. Treatment accuracy of fractionated stereotactic radiotherapy. *Radiother Oncol* 2005;74: 53–9.
13. Hurkmans CW, Remeijer P, Lebesque JV et al. Set-up verification using portal imaging; review of current clinical practice. *Radiother Oncol* 2001;58:105–20.
14. Pouliot J, Bani-Hashemi A, Chen J et al. Low-dose megavoltage cone-beam CT for radiation therapy. *Int J Radiat Oncol Biol Phys* 2005;61:552–60.
15. Li G, Ballangrud A, Kuo LC et al. Motion monitoring for cranial frameless stereotactic radiosurgery using video-based three-dimensional optical surface imaging. *Med Phys* 2011;38: 3981–94.
16. Inata H, Araki F, Kuribayashi Y et al. Development of a real-time monitoring system for intra-fractional motion in intracranial treatment using pressure sensors. *Phys Med Biol* 2015;60:7229–43.
17. Moore CJ, Amer A, Marchant T et al. Developments in and experience of kilovoltage X-ray cone beam image-guided radiotherapy. *Br J Radiol* 2006;79:S66–78.
18. Kamino Y, Takayama K, Kokubo M et al. Development of a four-dimensional image-guided radiotherapy system with a gimbaled X-ray head. *Int J Radiat Oncol Biol Phys* 2006;66: 271–8.
19. Walter C, Boda-Heggemann J, Wertz H et al. Phantom and *in-vivo* measurements of dose exposure by image-guided radiotherapy (IGRT): MV portal images vs. kV portal images vs. cone-beam CT. *Radiother Oncol* 2007;85:418–23.
20. Fallone BG, Murray B, Rathee S et al. First MR images obtained during megavoltage photon irradiation from a prototype integrated linac-MR system. *Med Phys* 2009;36:2084–8.
21. Farahmand F, Khadivi KO, Rodrigues JJ. Detecting intrafraction motion in patients undergoing radiation treatment using a low-cost wireless accelerometer. *Sensors (Basel)* 2009;9: 6715–29.
22. Peng JL, Kahler D, Li JG et al. Characterization of a real-time surface image-guided stereotactic positioning system. *Med Phys* 2010;37:5421–33.
23. Nath SK, Lawson JD, Wang J-Z et al. Optically-guided frameless linac-based radiosurgery for brain metastases: clinical experience. *J Neurooncol* 2010;97:67–72.
24. Takagi H, Obata Y, Kobayashi H et al. Clinical usefulness of a newly developed body surface navigation and monitoring system in radiotherapy. *J Appl Clin Med Phys* 2011;12:3400.
25. Bentel GC, Marks LB, Sherouse GW et al. A customized head and neck support system. *Int J Radiat Oncol Biol Phys* 1995;32: 245–8.
26. Chelvarajah R, Leighton B, Martin L. Cranial immobilisation—is there a better way? *Radiographer* 2004;51:29–33.
27. Fuss M, Salter BJ, Cheek D et al. Repositioning accuracy of a commercially available thermoplastic mask system. *Radiother Oncol* 2004;71:339–45.
28. Cerviño LI, Pawlicki T, Lawson JD et al. Frame-less and maskless cranial stereotactic radiosurgery: a feasibility study. *Phys Med Biol* 2010;55:1863–73.
29. Wang H, Wang C, Tung S et al. Improved setup and positioning accuracy using a three-point customized cushion/mask/bite-block immobilization system for stereotactic reirradiation of head and neck cancer. *J Appl Clin Med Phys* 2016;17: 180–9.
30. Kitahara T, Shirato H, Nishioka T et al. A new mold material for customized patient positioning in radiotherapy. *Radiother Oncol* 1998;47:77–9.
31. Fu D, Kuduvalli G. A fast, accurate, and automatic 2D–3D image registration for image-guided cranial radiosurgery. *Med Phys* 2008;35:2180–94.
32. Tominaga H, Araki F, Shimohigashi Y et al. Accuracy of positioning and irradiation targeting for multiple targets in intracranial image-guided radiation therapy: a phantom study. *Phys Med Biol* 2014;59:7753–66.

33. Kanda Y. Investigation of the freely available easy-to-use software 'EZR' for medical statistics. *Bone Marrow Transplant* 2013; 48:452–8.
34. Faul F, Erdfelder E, Lang A-G et al. G*Power: a flexible statistical power analysis program for the social, behavioral, and biomedical sciences. *Behav Res Methods* 2007;39:175–91.
35. Faul F, Erdfelder E, Buchner A et al. Statistical power analyses using G*Power 3.1: tests for correlation and regression analyses. *Behav Res Methods* 2009;41:1149–60.
36. Ali I, Tubbs J, Hibbitts K et al. Evaluation of the setup accuracy of a stereotactic radiotherapy head immobilization mask system using kV on-board imaging. *J Appl Clin Med Phys* 2010;11:3192.